HHS Public Access

Author manuscript

Angew Chem Int Ed Engl. Author manuscript; available in PMC 2017 February 12.

Published in final edited form as:

Angew Chem Int Ed Engl. 2016 February 12; 55(7): 2416–2420. doi:10.1002/anie.201509432.

Structurally-defined αMHC-II nanobody-drug conjugates: Therapeutic and imaging platforms for B-cell lymphoma

Dr. Tao Fang[a], **Joao N. Duarte**[a], **Jingjing Ling**[a,b], **Zeyang Li**[a,b], **Jonathan S. Guzman**[c], and **Prof. Hidde L. Ploegh**[a,c]

[a]Whitehead Institute for Biomedical Research, 9 Cambridge Center, Cambridge, MA 02142 (USA)

[b]Department of Biology, Massachusetts Institute of Technology, Cambridge, MA 02139

[c]Department of Chemistry, Massachusetts Institute of Technology, Cambridge, MA 02139

Abstract

Antibody-drug conjugates (ADCs) of defined structure hold great promise for cancer therapies, but further advances are constrained by the complex structures of full-sized antibodies. Camelid-derived single domain antibody fragments (VHHs or nanobodies) offer possible solutions to this challenge by providing expedited target screening/validation through shuttling between imaging and therapy. Here, we used a nanobody (VHH7) specific for murine MHC-II and rendered sortase-ready for introduction of oligoglycine-modified cytotoxic payloads or NIR fluorophores. The VHH7 conjugates outcompeted commercial mAbs for internalization and exhibited high specificity and cytotoxicity against the A20 murine B-cell lymphoma. Non-invasive NIR imaging with a VHH7-fluorophore conjugate showed rapid tumor targeting on both localized and metastatic lymphoma models. Subsequent treatment with the nanobody-drug conjugate efficiently controlled tumor growth and metastasis without obvious systemic toxicity.

Keywords

antibody–drug conjugates; sortase; nanobody; cancer

B-cell lymphoma is the most common type of non-Hodgkin's lymphoma (NHL). The American Cancer Society estimates that in 2015, ~70,000 new cases of NHL will be diagnosed in the United States, with mortality around ~20,000 patients. Antibodies against a variety of cellular receptors or antigens on B cells such as CD20,[1] surface immunoglobulins,[2] Class II major histocompatibility complex antigens (MHC-II),[3] CD80/CD86,[4] and CD40[5] have shown efficacy in treating B cell malignancies. The therapeutic mAb and ADC target CD20 (Rituximab) and CD30 (Brentuximab vedotin) represent a significant advance in the management of B cell malignancies.

Without exception, ADCs in the clinic so far rely on full-sized mAbs and on a rather limited range of conjugation methods, at times resulting in heterogeneous mixtures.[6] Accurate prediction of the drug:antibody ratio (DAR), crucial to the pharmaceutical properties of

Correspondence to: Hidde L. Ploegh.

ADCs and the translation of the manufacturing process from one antibody to another,[7] requires sophisticated mass spectroscopic methods and time-consuming empirical optimizations.[8] Recent efforts in making homogeneous ADCs[9] involve direct genetic approaches to install reactive cysteine residues,[10] unnatural amino acids,[11, 12] formylglycine-generating enzyme[13], or sortase[14] recognition motifs, or indirect glyco-[15, 16] or metabolic[17] engineering of the conserved N-glycan of the IgG Fc-domain. The structural complexity and post-translational modifications of mAbs complicate the straightforward expression and preparation of functionalized mAbs. To simplify mAbs while retaining essential functions, antibody fragments (scFv and Fab) and their engineered variants (diabodies, triabodies, minibodies) are the smaller format of choice.[18] Similar conjugation methods are generally transferable to antibody fragments. Their conjugates with radioactive tracers,[19, 20] nanomaterials,[21, 22] gene products,[23] immunomodulators,[24] cytotoxic reagents,[25, 26] or a combination[27] have demonstrated great maneuverability in therapeutic and diagnostic applications.

The discovery of unique heavy chain-only antibodies (HcAbs) in the family of *Camelidae*,[28] showed that their variable domains (VHHs), the smallest naturally derived antigen-binding fragment (~15KDa), retain antigen binding capacity when expressed recombinantly. The small size greatly benefits rapid circulatory clearance and reduces background in an non-invasive imaging setting.[19, 29] Their single domain nature allows convenient phagemid-based screening. The inherent absence of a hydrophobic surface that is usually present between V_H and V_L improves VHH solubility providing high yield (50 mg/L) in an *E. coli* expression system. No major framework rearrangements of VHHs have been observed, while the CDR3 domain is primarily involved in antigen binding and protrudes from the remaining binding surface, with the C-terminus extending in the opposite direction.[30] This justifies the installation of a C-terminal pentapeptide sortase recognition motif LPXTG, which, in turn, provides near limitless possibilities for site-specific modifications without compromising binding properties of the modified VHHs.[31–33] Collectively, nanobody-drug conjugates are desirable targets to develop the next generation of ADCs.[34]

We identified a VHH (VHH7) that binds murine class II major histocompatibility complex (MHC-II) molecules with low nM affinity. MHC-II is expressed on professional antigen presenting cells such as dendritic cells, B-cells, and macrophages. Compared to other B-cell markers like CD20, MHC-II is highly expressed on the B-cell surface ($8*10^4$ /cell for MHC-II v.s. $9*10^3$ /cell for CD20) [35, 36] and can be upregulated by antibody (rituximab) or immunostimulants such as CpG,[37] or IFN-γ[38]. Single agent therapy using two courses of Rituximab allows the outgrowth of CD20 loss variants in NHL patients, indicating a need for complimentary targets.[39]

We report here the preparation of a structurally defined nanobody-drug conjugate (VHH7-DM1) using sortase-mediated site-specific protein engineering, its pharmacokinetics and *in vivo* targeting as corroborated by non-invasive optical imaging. We show a therapeutic benefit of this conjugate by treating both a localized and a disseminated murine B-cell lymphoma, using the A20 cell line as a model.

To prepare a structurally defined VHH7-drug conjugate, we chose a thio-containing Maytansine derivative, Mertansine (DM1), as our cytotoxic payload. DM1 is a potent inhibitor of microtubule polymerization that has no useful therapeutic window when used as a single agent, but has been used to create ADCs.[40] Studies of Trastuzumab-emtansine (Kadcyla) showed that conjugation of DM1 to mAbs through a non-cleavable succinimidyl 4-(*N*-maleimidomethyl)cyclohexane-1-carboxylate (SMCC) linker, followed by the proteolytic degradation of this construct in endosomes/lysosomes, gave favorable clinical results in a phase III trial when compared to a cleavable disulfide linker.[41] Accordingly, we explored the sequential thiol-Michael ligation of a bis(maleimido)ethane (BMOE) linker[42] with the free mercapto group of hydrophilic peptide **1** and DM1 (Figure 1a). Using 5 equivalents of BMOE, peptide **1** is labeled monovalently and quantitatively after 16 h at room temperature in DMF. Excess BMOE was precipitated by the addition of water and the reaction mixture was purified by RP-HPLC, lyophilized, then converted to **2** after reacting with 2 equivalents of DM1 to give 80% conversion after 16 h, based on the integration of the HPLC trace. The sortase reaction between VHH7 and **2** was carried out following established protocols[43, 44] in which unreacted VHH7 and sortase were removed by incubation with Ni-NTA agarose beads, leaving product **3** and excess nucleophile **2**, which were easily separated by size exclusion chromatography (SEC) to obtain the desired product **3** . Identity of the conjugate was confirmed by LC-MS (Figure 1b) and when analyzed by SDS-PAGE the product yielded a single band (Figure 1c).

We also modified VHHs with a NIR dye, Alexa Fluor 647 (AF647) through sortagging. Binding of VHH7 to MHC-II positive A20 cells was measured at various concentrations of VHH7-AF647 and assessed by flow cytometry, showing half maximal binding (EC_{50}) at 2.1 nM (Figure 2a). Kinetics of VHH7 internalization were determined by incubation of A20 cells with VHH7-AF647, a genetic dimer of VHH7 labelled with AF647, a commercial anti-I-A/E IgGκ-AF488, and an irrelevant anti-human integrin VHH (2B7), followed by surface staining with anti-IgG-AF591 and analysis by confocal microscopy (Figure S3). Monovalent VHH7-AF647 was internalized within 1 h, while the internalization of the commercial anti-I-A/E reagent was observed only after overnight incubation. We tested the internalization of a bivalent format of VHH7, which is a tandem N to C arrangement of two VHH7 units with a single C-terminal AF647. A similar rate of internalization was observed for the dimer when applied at the same concentration. We performed a competition study by co-incubation of A20 cells with VHH7-AF647 and anti-I-A/E IgGκ-AF488, and saw that VHH7 was internalized rapidly and appeared in vesicular structures within 5 min, leaving the commercial anti-I-A/E reagent visible as a rim stain (Figure 2b). The rapid internalization of VHH7 upon binding to MHC-II suggested its use for targeted drug delivery. In contrast, CD20 is not internalized as rapidly, making it a better mediator of ADCC.[45] An anti-EGFR nanobody also showed slow internalization.[46]. The choice of target as it relates to its internalization is thus an important parameter in the design of VHH-drug conjugates.

We studied the *in vitro* cytotoxicity of the VHH7-DM1 conjugate against the murine lymphoma A20, and MHC-II negative cell lines such as HeLa and HEK293 (Figure 2c, S2). Cells (4×10^4 per well in a 96 well plate) were exposed to VHH7-DM1 or to unconjugated DM1 at increasing concentrations. The VHH-DM1 fusion effectively killed A20 cells with

an IC_{50} = 36 nM; however, HeLa and HEK293 required ~500 nM (Figure S2), demonstrating the selective action of the VHH-DM1 fusion. The unconjugated drug shows similar cytotoxicity for all three cell lines.

We confirmed systemic targeting against A20 lymphoma in both localized and metastatic models by non-invasive optical imaging. We detected the subcutaneous tumor after i.v. injection of VHH7-AF647 as monitored by IVIS (Figure 3a,b). Injection of an irrelevant nanobody-AF647 conjugate (Enh-AF647) into an A20 -bearing mouse, or injection of VHH-AF647 into a MHC-II KO mouse resulted in rapid clearance without signs of non-specific binding at the tumor site. The average radiant efficiency of the tumor and the S/N ratio at different time points (Figure S6) suggested that *in vivo* targeting reached a maximum at 30 min and persisted over the next 96 h. The signal from the kidney reached its maximum within 5 h and then progressively decreased, consistent with kidneys being the major clearance pathway for VHHs.[47] Targeting at the cellular level was also confirmed when tumors were removed 2 h p.i. of VHH7-AF647 compared to Enh-AF647, frozen, sectioned, and mounted for confocal microscopy (Figure S4). Vesicular structures were observed for samples from VHH7-AF647 injected mice, while no signal was detected for Enh-AF647.

Lung, liver, spleen and lymph nodes are all possible sites of invasion in the case of disseminated lymphoma. We observed strong signals from the lungs and liver by NIR imaging (Figure 3c, d), whereas signals from healthy Balb/c mainly emanated from the GI tract and bladder. To confirm targeting of VHH7 to metastatic foci, both healthy and tumor-bearing mice were injected with 40 μg VHH7-AF647, dissected, followed by comparison of fluorescent signals from lung, liver and spleen (Figure 3e). The presence of lymphoma in these organs was first confirmed cytologically. Metastasic foci were found in liver, with splenomegaly as a consequence of tumor infiltration. NIR-imaging was consistent with the cytological observations: all tumor-bearing organs showed strong fluorescent signals. The fluorescent signal persists even after 24 h, owing to retention of VHH7 at the tumor site, with delayed clearance compared to healthy mice (Figure 3f,g). A meaningful comparison of the biodistribution of VHH7 and full-sized αI-A/E would require a full-sized Ab of the identical specificity and labelled to the same intensity, a preparation that we currently lack. VHH7 is monovalently labelled, while the full-sized α-I-A/E has 8~10 fluorophores per molecule. When VHH7 and full-sized α-I-A/E were injected at the same fluorescent dose, a stronger signal was seen for VHH7 at the tumor site (Figure 3h). Injection of similar molar quantities of VHH7 and full-sized α-I-A/E showed increased staining of VHH7 for spleen and inguinal lymph nodes comparing to α-I-A/E (Figure S8).

Finally, the VHH7-DM1 conjugate was subjected to tests *in vivo* to treat the highly invasive A20 lymphoma, known to target spleen, liver and lymph nodes. The A20 tumors are radioresistant at myeloablative doses of radiation and only poorly immunogenic. Neither radiation nor vaccine therapy affords protection.[48] We first engrafted A20 subcutaneously to monitor the progression of a single tumor at a known site. The tumors were allowed to grow until the average volume reached 150 mm^3. Starting at day 10 p.i., a total of 5 doses of VHH7-DM1 at 125 μg/injection (5 mg/kg) were administered every other day, with daily monitoring of tumor size (Figure 4a). Final sizes of tumors in the VHH7-DM1 treated group remained significantly smaller than those in the PBS-treated control [mean: 1479 mm^3

(controls) *v.s.* 480 mm^3 (VHH7-DM1 treated), $p = 0.012$, n=3]. Mice treated with VHH7 alone were no different from the controls ($p = 0.99$). We next explored the disseminated A20 model. After i.v injection of A20 cells, treatment started the next day at 125 μg/injection (5 mg/kg) every other day for a total of 4 injections. Mice were sacrificed on day 27 when metastatic foci in the livers of the control group became palpable. We enumerated the liver foci for untreated and VHH7/Enh-DM1 treated groups (Figure 4b). The efficacy of VHH7-DM1 in limiting metastasic spread is encouraging, in that no more than 3 small foci (Φ < 3mm) were found for the treated group. In untreated animals and in the Enh-DM1 treated group, massive liver metastases [liver weight = 4.8 ± 0.87 g (mean ± SD), n = 5, normal weight ~1.4 g] were seen, with up to 30 foci. Survival was monitored in a parallel experiment (Figure S7). After 4 injections, VHH7-DM1-treated mice showed increased median survival of 44 days, compared to 29 days for animals treated with Enh-DM1. No nephrotoxicity was observed after 6 injections, as inferred from creatinine levels [0.27 ± 0.06 mg/ml (mean ± SD), n=3, normal range 0~1 mg/ml]. Injection of healthy mice with two doses of VHH7-DM1, followed by analysis of splenocytes by FACS analysis 5 days later did not show significant differences in MHC-II^+ populations [$CD19^+$ (B-cells): 52.1% v.s. 51.3%; $CD11b^+CD11c^-$ (macrophages): 1.7% v.s. 1.6%; $CD11b^+CD11c^+$(DCs): 0.4% v.s. 0.3%; control v.s. injection; average of two].

In summary, we generated a homogeneous anti-MHC-II nanobody-drug conjugate (VHH7-DM1) through SrtA-mediated protein conjugation. The conjugate was characterized *in vivo* and *in vitro* and was efficient in treating an aggressive murine B-cell lymphoma. The favorable pharmacokinetics of VHH conjugates outcompete commercial mAbs for internalization and clearance providing reduced systemic cytotoxicity and convenient non-invasive imaging.

Supplementary Material

Refer to Web version on PubMed Central for supplementary material.

Acknowledgments

This research was supported by NIH (R01AI087879) and NIH DP1. We thank the Whitehead Institute flow cytometry facility, W. M. Keck biological imaging facility (N. Watson and W. Salmon) and Preclinical Imaging Core of the Koch Institute (S. Malstrom) for instrument usage.

References

1. Shan D, Ledbetter Ja, Press OW. Blood. 1998; 91:1644–1652. [PubMed: 9473230]
2. Mayumi M, Sumimoto S, Kanazashi S, Hata D, Yamaoka K, Higaki Y, Ishigami T, Kim KM, Heike T, Katamura K. J. Allergy Clin. Immunol. 1996; 98:S238–S247. [PubMed: 8977533]
3. Dechant M, Bruenke J, Valerius T. Semin. Oncol. 2003; 30:465–475. [PubMed: 12939715]
4. Yang Z-Z, Novak AJ, Ziesmer SC, Witzig TE, Ansell SM. Cancer Res. 2009; 69:5522–5530. [PubMed: 19509224]
5. von Bergwelt-Baildon M. Ann. Oncol. 2004; 15:853–857. [PubMed: 15151939]
6. Mullard A. Nat. Rev. Drug Discov. 2013; 12:329–332. [PubMed: 23629491]
7. Shen B-Q, Xu K, Liu L, Raab H, Bhakta S, Kenrick M, Parsons-Reponte KL, Tien J, Yu S-F, Mai E, et al. Nat. Biotechnol. 2012; 30:184–189. [PubMed: 22267010]
8. Goldmacher VS, Amphlett G, Wang L, Lazar AC. Mol. Pharm. 2015 150217101755004.

9. Agarwal P, Bertozzi CR. Bioconjug. Chem. 2015; 26:176–192. [PubMed: 25494884]
10. Junutula JR, Raab H, Clark S, Bhakta S, Leipold DD, Weir S, Chen Y, Simpson M, Tsai SP, Dennis MS, et al. Nat. Biotech. 2008; 26:925–932.
11. Kularatne, Sa, Deshmukh, V., Ma, J., Tardif, V., Lim, RKV., Pugh, HM., Sun, Y., Manibusan, A., Sellers, AJ., Barnett, RS., et al. Angew. Chem. Int. Ed. 2014; 53:11863–11867.
12. Axup JY, Bajjuri KM, Ritland M, Hutchins BM, Kim CH, Kazane Sa, Halder R, Forsyth JS, Santidrian AF, Stafin K, et al. Proc. Natl. Acad. Sci. 2012; 109:16101–16106. [PubMed: 22988081]
13. Agarwal P, van der Weijden J, Sletten EM, Rabuka D, Bertozzi CR. Proc. Natl. Acad. Sci. 2013; 110:46–51. [PubMed: 23237853]
14. Beerli RR, Hell T, Merkel AS, Grawunder U. PLoS One. 2015; 10:e0131177. [PubMed: 26132162]
15. Li X, Fang T, Boons GJ. Angew. Chem. Int. Ed. 2014; 53:7179–7182.
16. Smith EL, Giddens JP, Iavarone AT, Godula L-X, Wang K, Bertozzi CR. Bioconjug. Chem. 2014; 25:788–795. [PubMed: 24702330]
17. Okeley NM, Toki BE, Zhang X, Jeffrey SC, Burke PJ, Alley SC, Senter PD. Bioconjug. Chem. 2013; 24:1650–1655. [PubMed: 24050213]
18. Holliger P, Hudson PJ. Nat. Biotechnol. 2005; 23:1126–1136. [PubMed: 16151406]
19. Freise AC, Wu AM. Mol. Immunol. 2015; 67:142–152. [PubMed: 25934435]
20. Massa S, Xavier C, De Vos J, Caveliers V, Lahoutte T, Muyldermans S, Devoogdt N. Bioconjug. Chem. 2014; 25:979–988. [PubMed: 24815083]
21. Chen G-Y, Li Z, Theile CS, Bardhan NM, Kumar PV, Duarte JN, Maruyama T, Rashidfarrokh A, Belcher AM, Ploegh HL. Chem. Eur. J. 2015
22. Ahn J, Miura Y, Yamada N, Chida T, Liu X, Kim A, Sato R, Tsumura R, Koga Y, Yasunaga M, et al. Biomaterials. 2015; 39:23–30. [PubMed: 25477168]
23. Sadeqzadeh E, Rahbarizadeh F, Ahmadvand D, Rasaee MJ, Parhamifar L, Moghimi SM. J. Control. Release. 2011; 156:89–95.
24. Pasche N, Neri D. Drug Discov. Today. 2012; 17:583–590. [PubMed: 22289353]
25. Cao Y, Marks JW, Liu Z, Cheung LH, Hittelman WN, Rosenblum MG. Oncogene. 2014; 33:429–439. [PubMed: 23376850]
26. Kim KM, McDonagh CF, Westendorf L, Brown LL, Sussman D, Feist T, Lyon R, Alley SC, Okeley NM, Zhang X, et al. Mol. Cancer Ther. 2008; 7:2486–2497. [PubMed: 18723494]
27. List T, Casi G, Neri D. Mol. Cancer Ther. 2014; 13:2641–2652. [PubMed: 25205656]
28. Hamers-Casterman C, Atarhouch T, Muyldermans S, Robinson G, Hammers C, Songa EB, Bendahman N, Hammers R. Nature. 1993; 363:446–448. [PubMed: 8502296]
29. Rashidian M, Keliher EJ, Bilate AM, Duarte JN, Wojtkiewicz GR, Jacobsen JT, Cragnolini J, Swee LK, Victora GD, Weissleder R, et al. Proc. Natl. Acad. Sci. 2015; 112:6146–6151. [PubMed: 25902531]
30. Desmyter A, Transue TR, Ghahroudi MA, Dao Thi M-H, Poortmans F, Hamers R, Muyldermans S, Wyns L. Nat. Struct. Biol. 1996; 3:803–811. [PubMed: 8784355]
31. Popp MW, Antos JM, Grotenbreg GM, Spooner E, Ploegh HL. Nat. Chem. Biol. 2007; 3:707–708. [PubMed: 17891153]
32. Li Z, Theile CS, Chen G-Y, Bilate AM, Duarte JN, Avalos AM, Fang T, Barberena R, Sato S, Ploegh HL. Angew. Chem. Int. Ed. 2015; 127:11872–11876.
33. Witte MD, Cragnolini JJ, Dougan SK, Yoder NC, Popp MW, Ploegh HL. Proc. Natl. Acad. Sci. 2012; 109:11993–11998. [PubMed: 22778432]
34. Kijanka M, Dorresteijn B, Oliveira S, van Bergen en Henegouwen PM. Nanomedicine. 2015; 10:161–174. [PubMed: 25597775]
35. Demotz S, Grey HM, Sette A. Science. 1990; 249:1028–1030. [PubMed: 2118680]
36. Ginaldi L, De Martinis M, Matutes E, Farahat N, Morilla R, Catovsky D. J. Clin. Pathol. 1998; 51:364–369. [PubMed: 9708202]

37. Jahrsdörfer B, Hartmann G, Racila E, Jackson W, Mühlenhoff L, Meinhardt G, Endres S, Link BK, Krieg aM, Weiner GJ. J. Leukoc. Biol. 2001; 69:81–88. [PubMed: 11200072]
38. Zhao M, Flynt FL, Hong M, Chen H, Gilbert CA, Briley NT, Bolick SC, Wright KL, Piskurich JF. Mol. Immunol. 2007; 44:2923–2932. [PubMed: 17300840]
39. Davis, Ta, Czerwinski, DK., Levy, R. Clin. Cancer Res. 1999; 5:611–615. [PubMed: 10100713]
40. Tan, C. Antibody-Drug Conjug. SE - 2. Wang, J.Shen, W-C., Zaro, JL., editors. Springer International Publishing; 2015. p. 11-22.
41. Erickson HK, Park PU, Widdison WC, Kovtun YV, Garrett LM, Hoffman K, Lutz RJ, Goldmacher VS, Blattler WA. Cancer Res. 2006; 66:4426–4433. [PubMed: 16618769]
42. The degradation of thiol-Micheal adducts has been reported; however, this process is generally slow when compared to the clearance of VHHs. The improvement in stability is referred to in comparison with disulfide or hydrazone linkers.
43. Theile CS, Witte MD, Blom AEM, Kundrat L, Ploegh HL, Guimaraes CP. Nat. Protoc. 2013; 8:1800–1807. [PubMed: 23989674]
44. Guimaraes CP, Witte MD, Theile CS, Bozkurt G, Kundrat L, Blom AEM, Ploegh HL. Nat. Protoc. 2013; 8:1787–1799. [PubMed: 23989673]
45. Boross P, Leusen JHW. Am. J. Cancer Res. 2012; 2:676–690. [PubMed: 23226614]
46. Heukers R, van Bergen en Henegouwen PMP, Oliveira S. Nanomedicine Nanotechnology, Biol. Med. 2014; 10:1441–1451.
47. De Vos J, Devoogdt N, Lahoutte T, Muyldermans S. Expert Opin. Biol. Ther. 2013; 13:1149–1160. [PubMed: 23675652]
48. Graner M, Raymond A, Romney D, He L, Whitesell L, Katsanis E. Clin. Cancer Res. 2000; 6:909–915. [PubMed: 10741715]

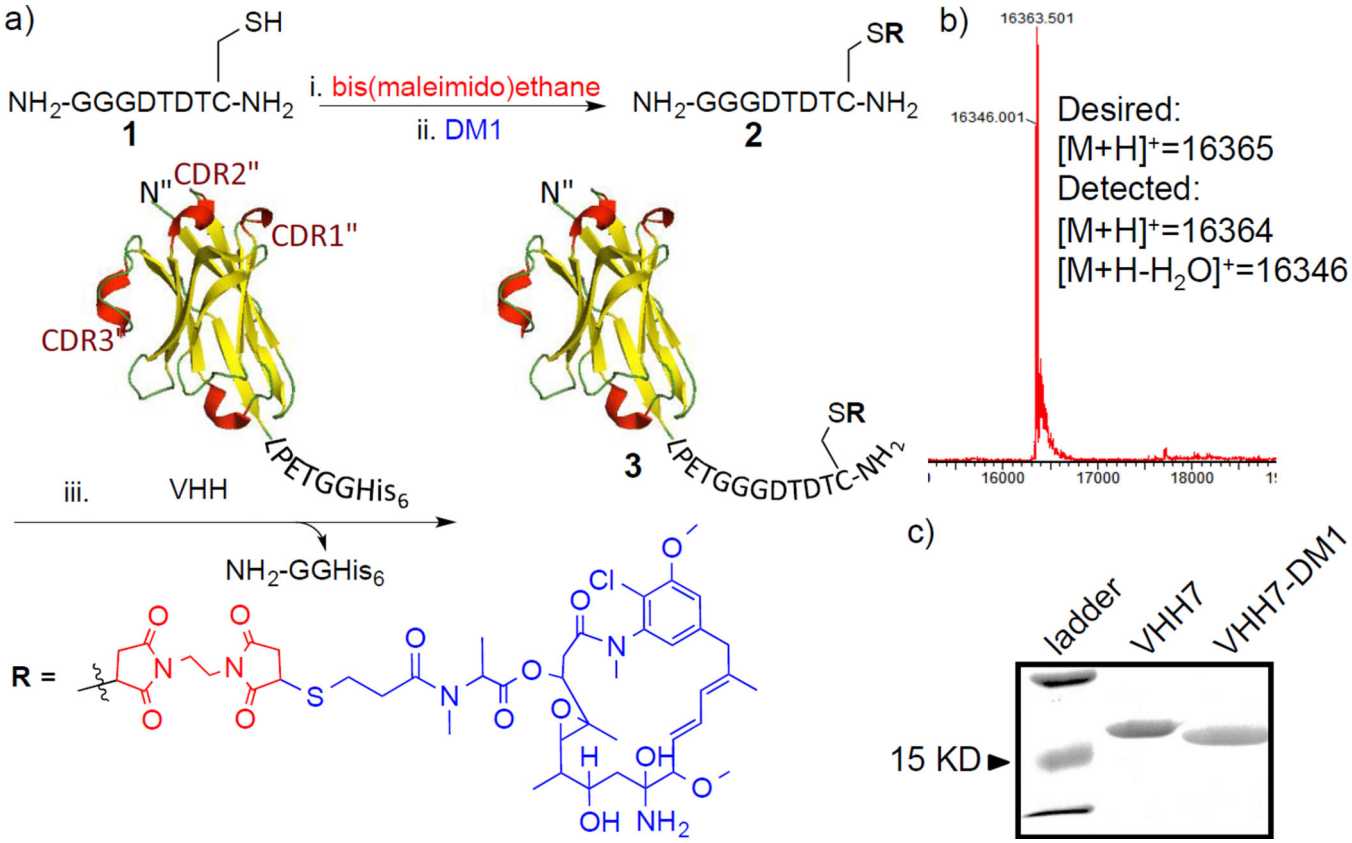

Figure 1.

Synthesis and characterization of structurally defined VHH7-DM1 conjugate. a) Preparation of VHH7-DM1 conjugate. Conditions: i) DMF, r.t. 2 h; ii) DMF/PBS = 4/1 (v/v), 18 °C, 16 h; iii. Srt A (pentamutant), 10mM $CaCl_2$, 50 mM Tris, pH = 7.4, 12 °C, 2~4 h; b) LC-MS analysis of VHH7-DM1; c) SDS-PAGE analysis of VHH7-DM1 conjugate (15% gel, InstantBlue, faster mobility of VHH7-DM1 was due to the cyclic structure of DM1, LC-MS profile attached in Fig. S1c).

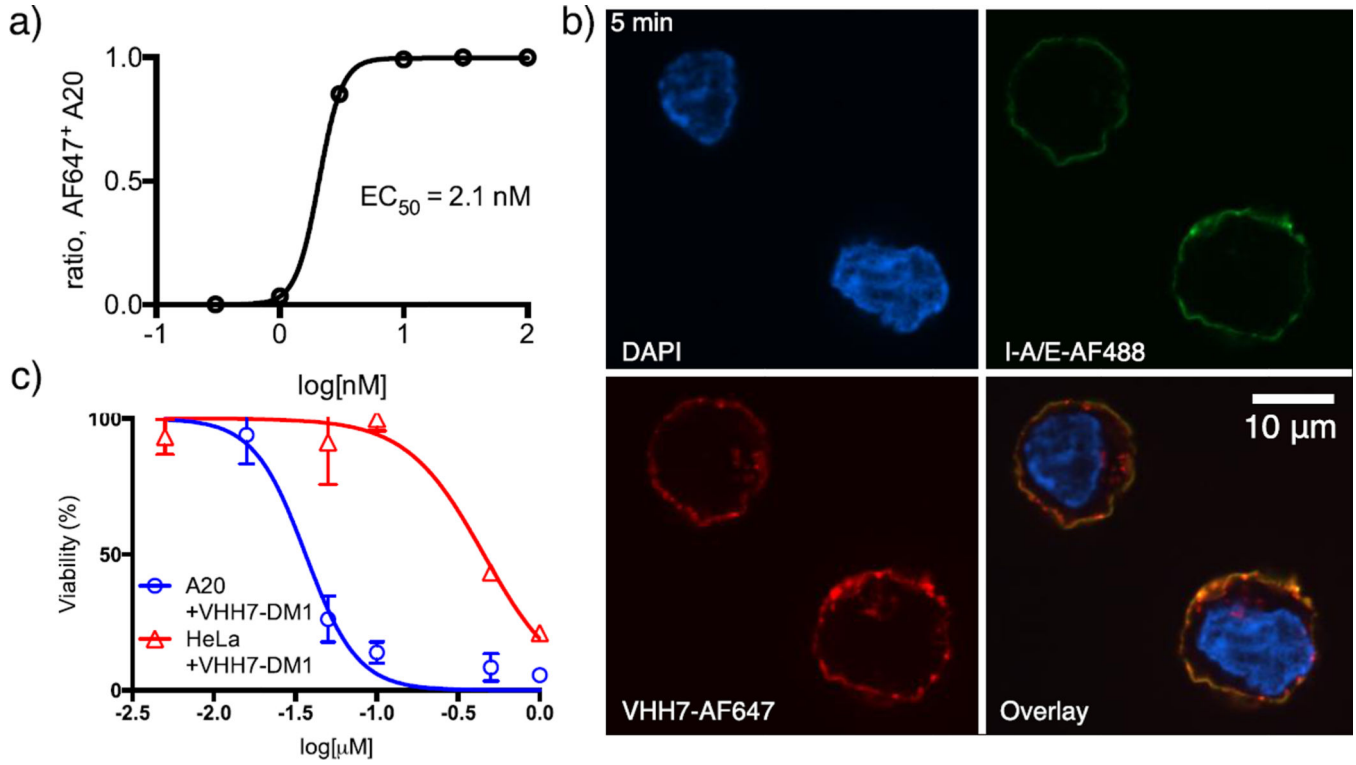

Figure 2.

In vitro characterization of VHH7 conjugates. a) Half maximal effective binding of VHH7-AF647 to murine lymphoma A20 cells. 5×10^5 cells were incubated with increasing concentration of VHH7-AF647 at 4 °C for 1 h, then washed 3 times and analyzed by flow cytometry. b) Internalization of commercial antibody anti-I-A/E-AF488 (M5/114.15.2) and VHH7-AF647. Equal molar amount of VHH-AF647 and anti-I-A/E-AF488 were premixed and added to cells in poly-L-lysine coated imaging chamber at final concentration of 50 nM. After 5 min, cells were washed with ice-cold PBS, then fixed and mounted for confocal microscopy. c) *In vitro* cytoxocity of VHH7-DM1 conjugate on MHC-II positive (A20) and negative cell lines (Hela) (n=3, bars, means ± SD).

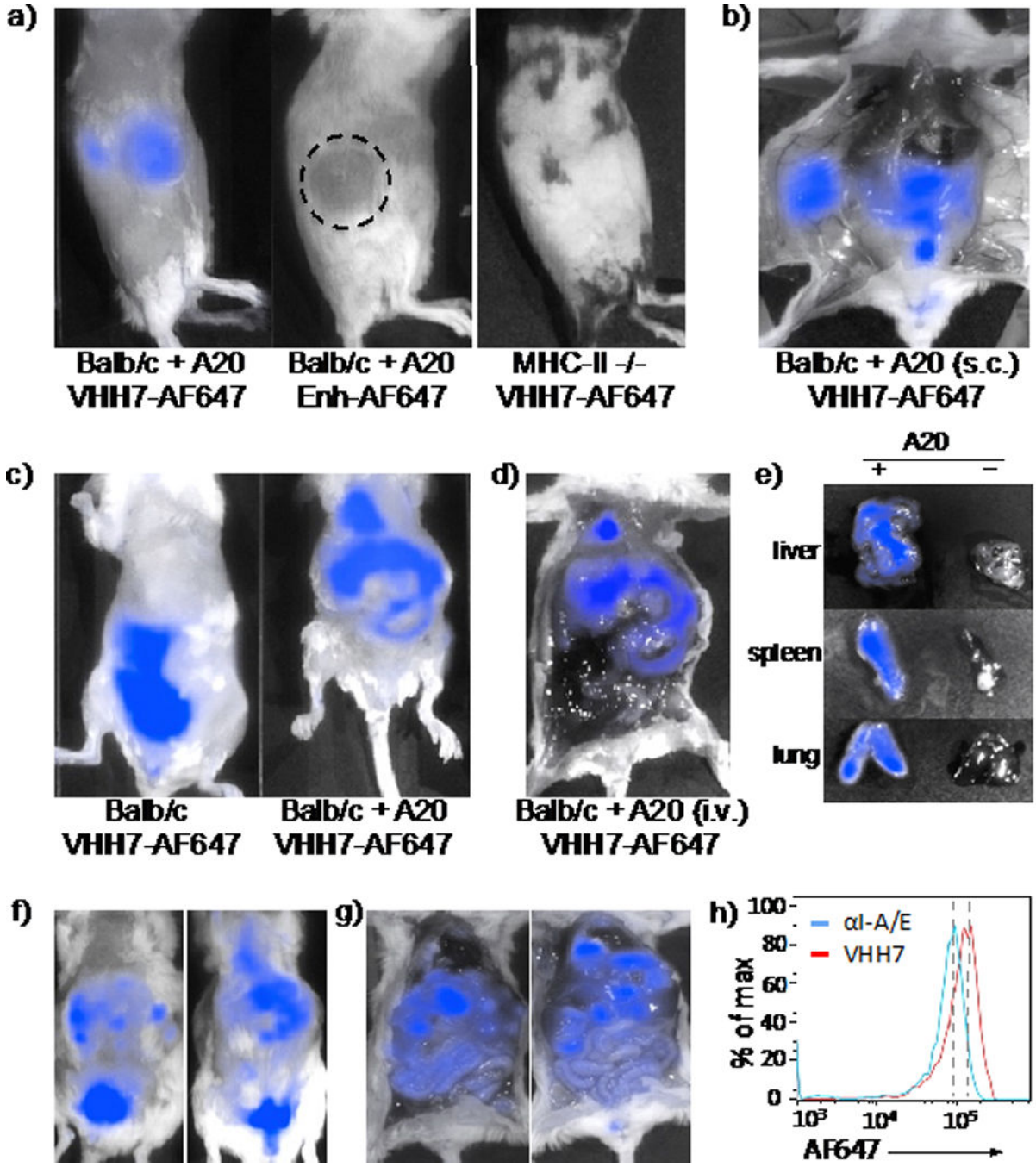

Figure 3.

Non-invasive NIR imaging of A20 lymphoma by VHH7-AF647 conjugate. (color scale: full range, minimum to maximum). a) Balb/c with subcutaneous A20 (left, middle) and MHC-II KO (right) were injected with 40 μg VHH7-AF647 or irrelevant Enhancer-AF647 conjugate as denoted, then imaged on IVIS. Pictures show 5 h p.i. (black dashed circle highlights tumor burden); b) Mouse with subcutaneous A20 was dissected 16 h p.i. of VHH7-AF647 to show clear tumor targeting; c) Healthy (left) and A20 intravenously inoculated (right, 4 weeks p.i.) Balb/c were imaged 5 h p.i. of VHH7-AF647; d) Mouse with metastatic A20 was

dissected 5 h p.i. of VHH7-AF647 injection to show clear tumor targeting on lung, liver and spleen; e) Organs from metastatic and healthy mice (panel c) were imaged in the same view; f) Two Balb/c mice with disseminated A20 lymphoma (4 weeks after inoculation) were imaged 24 h p.i. of VHH7-AF647; g) Mice from panel f were dissected to show targeting at tumor sites. h) Comparable doses (6400 RFU) of fluorescently labeled VHH7-AF647 and α-I-A/E-AF647 were injected into mice bearing subcutaneous tumors. The tumors were removed and analyzed by FACS. Shift in mean fluorescence intensity: 92K(I-A/E) to 135K (VHH7).

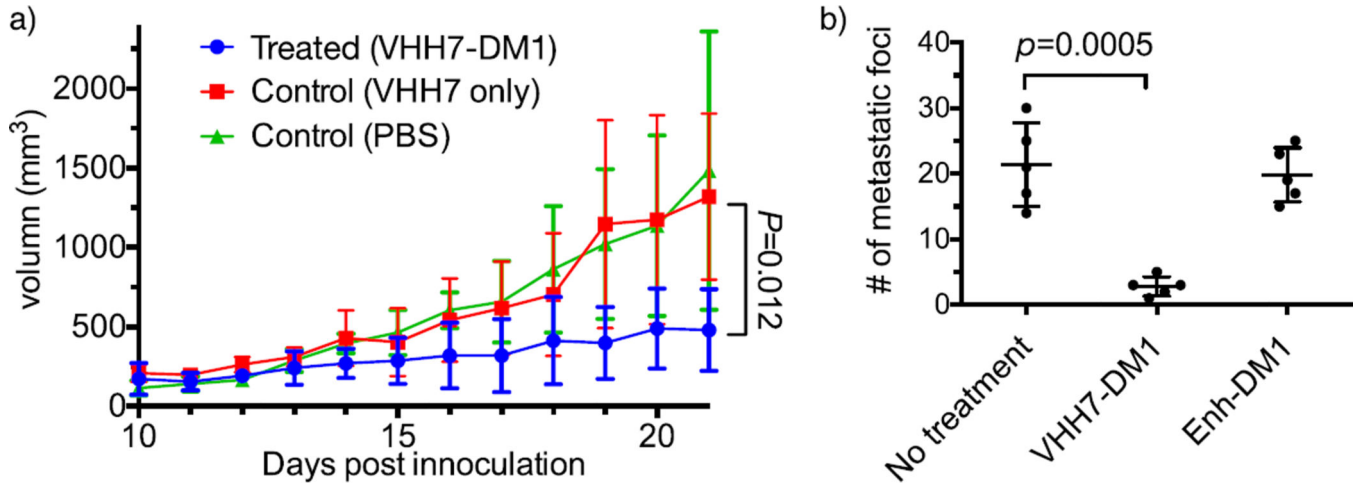

Figure 4.

In vivo efficiency of VHH7-DM1 conjugate in treating A20 lymphoma. a) VHH7-DM1 conjugate inhibited tumor growth in a localized model. 9 Balb/c were inoculated with 2.5×10^6 A20 cells subcutaneously then randomized into 3 groups at day 10 when tumor burdens became measurable by caliper. Starting at day 10, samples were given i.v. at dose of 125 μg/mice (5 mg/kg for 25 g mice) and followed every other day for a total of 5 injections. Tumor volume (V) was used to evaluate tumor size using a modified ellipsoid formula: $V = (\text{width})^2 \times \text{length} / 2$ (Bars, means ± SD, n = 3). Experiment end point was defined as when the largest single tumor size exceeded 2000 mm^3. b) VHH7-DM1 protected mice from tumor metastasis in a disseminated model. 15 Balb/c were inoculated with 1.5×10^6 A20 subcutaneously, then randomized into 3 groups. Injection started at day 2 with a dose of 125 μg/mice and followed every other day for a total of 4 injections. Mice were sacrificed on day 27, and the number of metastatic foci on liver was counted (Bars, means ± SD, n = 5).